Non-linear bubbly Helmholtz resonator

Matthieu Malléjac, Cédric Payan, Lilian d'Hondt, Serge Mensah, Aroune Duclos, Matthieu Cavaro

Non-linear Bubbly Helmholtz Resonator

Matthieu MALLÉJAC[1,3], Cédric PAYAN[2], Lilian D'HONDT[1,2], Serge MENSAH[2], Aroune DUCLOS[3], Matthieu CAVARO[1]

[1] CEA, DES IRESNE, DTN/STCP/Laboratory of Instrumentation, Systems and Methods - 13115 St Paul Les Durance, France

[2] Aix-Marseille Univ, CNRS, Centrale Marseille, LMA, Marseille, France

[3] Laboratoire d'Acoustique de l'Université du Mans - UMR 6613 CNRS - Le Mans Université, 72085 Le Mans Cedex 09, France

Abstract

Microbubble clouds greatly affect the acoustic behaviour of systems such as liquid-filled Helmholtz resonators. Gas microbubbles change the resonator's behaviour from quasi-linear to mostly non-linear, together with the appearance of hysteretic phenomena and desymmetrisation of the temporal response or a softening effect with a drop in the resonance frequencies with increasing excitation amplitudes. The aim of this study is to model the non-linear behaviour of a diphasic Helmholtz resonator filled with water containing air microbubbles. The microbubble cloud is therefore modelled with a "damped-mass-spring" second-order equation. The impact of the two phases is accounted for by considering both an equivalent stiffness and an equivalent damping value. The model is then compared to experimental data, which showed its ability to reproduce both linear and non-linear behaviour.

Nonlinear Resonant Acoustic Spectroscopy, Two-phase, Helmholtz Resonator, Bubble cloud, Void fraction, Microbubble

1. Introduction

In a context where the global electricity demand continues to increase, the French Atomic Energy and Alternative Energies Commission (CEA) conducts research on the development of sodium-cooled fast nuclear reactors (SFR) within the scope of the Generation IV International Forum (GIF).

As liquid sodium is opaque, acoustic non-destructive testing (NDT) and sodium viewing methods have to be developed, which requires accurate knowledge of liquid sodium's physical properties. The presence of argon gaseous microbubbles in the liquid sodium - mainly due to nucleation and gas entrainment - largely modifies its compressibility and celerity. This has led to the development of bubbly liquid characterisation techniques to evaluate both the void fraction τ, which represents the ratio of the gas volume to the total volume, and the cloud histogram, which refers to the distribution of bubble radii.

Different bubble cloud characterisation methods exist [1]. The CEA has focused its research on acoustic techniques, such as mixing frequency techniques [2], attenuation and velocity spectroscopy [3], and low-frequency acoustic velocity measurements (LF-AVM) [4].

Another way of characterising a bubbly liquid is to confine the micro-bubble cloud in a resonator and to study the impact of the two-phase medium on the resonance. Both the linear and non-linear resonant behaviour of the system depends on the properties of the cloud. First, an estimate of the void fraction and the mean bubble radius can be made in the linear regime (small excitation amplitudes). The resonance frequency of the system can be compared with that predicted either by Wood's model, which couples the speed of sound (and thus the system's resonance frequency) and the void fraction [5], or by Prosperetti's model, which includes the impact of radii [6]. Second, a softening effect, *i.e.*, a decrease in resonance frequency with increasing excitation amplitude, can be observed in the non-linear regime [12].

Characterisation techniques based on this softening effect, such as the Non-linear Resonant Acoustic Spectroscopy (NRAS), have been developed to assess the fatigue of rocks and concrete [9-11] and might be transposed to the characterisation of bubble clouds. This method consists in representing the relative variation of the resonance frequency as a function of the excitation amplitude. Three zones can generally be observed: a linear zone with an almost zero variation of the resonance frequency, followed by a quadratic evolution and finally a linear variation of the resonance frequency, whose slope is quantified according to the properties of the media (fatigue state and microcracks in the case of concrete [9-11]). However, to the best of our knowledge, the physical parameters cannot yet be determined on the basis of this information. Some experimental NRAS tests on bubbly liquids [12, 13] have been undertaken without further characterisation.

The absence of an analytical modelling of such two-phase resonators prevents a thorough investigation of the influence of each of the bubble cloud parameters on the NRAS technique. To fill this gap, we propose to model in this study a two-phase Helmholtz resonator, capable of reproducing both linear and non-linear resonant behaviour observed experimentally.

The paper is organized as follows. We first expose the proposed model derivation, before providing analytical results to validate its linear resonant response with Wood's and Prosperetti's well-known effective medium models. The third part of the study compares the model with the experimental results. Future prospects are then discussed in the conclusion.

2. Theoretical background

As two-phase medium compressibility is highly sensitive to void fractions, this property is used as the basis for our model. Moreover, since the behaviour of both microbubbles and Helmholtz resonators can be modelled by an analogue damped-mass-spring system [14-16], the two-phase Helmholtz resonator is modelled likewise.

We adopt here a macro-micro description of the two-phase Helmholtz resonator. The entire system is described as an effective medium (macroscopic view), the properties of which are directly derived from the microbubble reaction to an external excitation (microscopic view).

We then adopt first a macroscopic description to model the response of the effective two-phase Helmholtz resonator.

The system's behaviour can be described as the displacement of a fluid mass in the neck of length L_{neck} resulting from an excitation pressure P, applied to the opening of the Helmholtz resonator with a cross-section $S_m = \pi R_m^2$ and a cavity volume V_c as shown in Fig. 1.

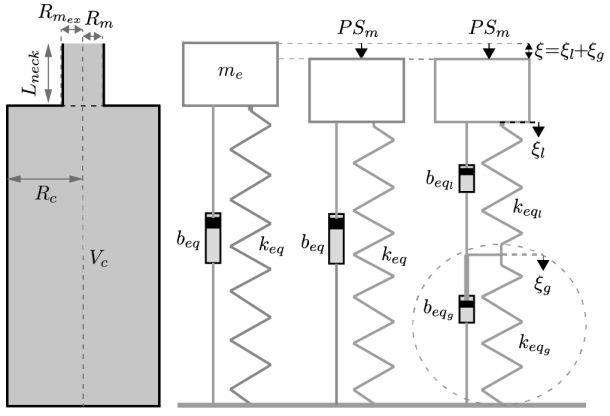

Figure 1: Two-phase Helmholtz resonator modelled as a damped mass spring system

The fluid mass displacement ξ in the resonator neck is governed by a second-order differential equation such as

$$m_{eff}\ddot{\xi} + b_{eq}\dot{\xi} + k_{eq}\xi = PS_m e^{i\omega t}, \quad (1)$$

with ω the excitation pulsation. The effective mass of moving fluid in the neck of length L_{neck}, $m_{eff} = \rho_{eff} S_m L_e$, accounts for the radiation at the openings by considering an effective length L_e. Cummings [17]

recommends using an end correction corresponding to that of a semi-infinite tube [18] for the mouth L_{end_m} and to that of an infinite baffled piston [19] for the opening to the resonator cavity L_{end_c}, *i.e.*,

$$\begin{aligned} L_e &= L_{neck} + L_{end_m} + L_{end_c} \\ &= L_{neck} + \frac{8}{3\pi} R_c + \frac{d_m}{d_{m_{ex}}} R_m \end{aligned} \tag{2}$$

where $d_m = 2R_m$ is the internal opening diameter, $d_{m_{ex}}$ is the external diameter, and R_c is the cavity radius. The equivalent stiffness k_{eq} and damping b_{eq} are defined in sub-sections 2.1 and 2.2 respectively.

Based on the elementary Helmholtz resonator model, the stiffness k_{eq} of the two-phase resonator creates a restoring force at the mouth's cross-section S_m. The bubble population, which has its own compressibility, also acts on this restoring force.
We then adopt a microscopic view to derive these equivalent properties from the microbubble cloud as schemed in Fig. 2. The polydisperse bubble population can be represented by a histogram (number of microbubbles versus bubble radii), which can be divided into several radius classes, w. Each population class gathers every single bubble whose radius falls in the range of the class.

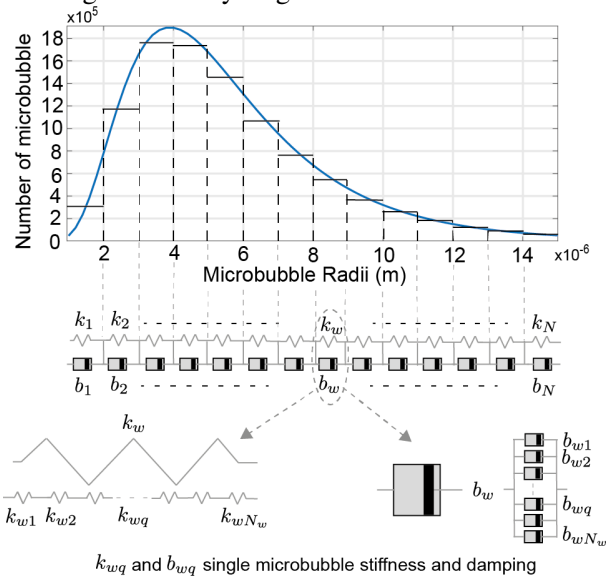

Figure 2: Microbubble population ($R = 1 - 15$ μm and $\tau = 10^{-4}$) modelled as a damped mass spring system

2.1. Equivalent stiffness

To derive the equivalent stiffness k_{eq} of the two-phase Helmholtz resonator, a series combination of the equivalent springs representing the equivalent stiffness of the gaseous phase $k_{eq,g}$ and stiffness of the liquid phase $k_{eq,l}$ is assumed (see Fig.1)

$$k_{eq} = \left[\frac{1}{k_{eq,g}} + \frac{(1-\tau)V_c\chi_l}{S_m^2}\right]^{-1}. \tag{3}$$

The equivalent stiffness of the gaseous phase, depicted in Fig. 2, results from a series combination of the stiffness of each radius range k_w and of the N_w identical microbubbles in the w^{th} class, k_{wq}, leading to

$$k_{eq\,g} = \left[\sum_w \frac{1}{k_w}\right]^{-1}, \tag{4}$$

with

$$k_w = \left[\sum_q^{N_w} \frac{1}{k_{wq}}\right]^{-1} = \frac{k_{wq}}{N_w}. \tag{5}$$

We assumed here that each bubble in the w^{th} class shares the same stiffness since the variation in volume is the same.

An elementary stiffness, modelled similarly to that of a spring [21], is assumed and assigned to each microbubble of the cloud

$$k = \frac{S_m^2}{\chi V_0}, \tag{6}$$

with the subscript $._{wq}$ omitted for readability.

The compressibility of each individual bubble of equilibrium radius R_0 from the population is determined by solving the Laplace equation, $PV^\kappa = const$, or

$$\left(P_{atm} + \frac{2\sigma}{R_0}\right) V_0^\kappa = \left(P_{atm} + P + \frac{2\sigma}{R}\right) V^\kappa, \tag{7}$$

so as to estimate the variation in the volume

$$\Delta V = V - V_0 = \frac{4\pi}{3}(R^3 - R_0^3), \tag{8}$$

and the variation in the internal pressure

$$\Delta P = P - P_0 = P_{atm} + 2\sigma\left(\frac{1}{R} - \frac{1}{R_0}\right), \tag{9}$$

where P_{atm} is the ambient pressure (atmospheric pressure), σ is the surface tension, $._0$ refers to steady state, and κ to the polytropic coefficient.

An isothermal behaviour is assumed considering that the average thermal penetration depth, $l_d = \sqrt{\frac{2D_g}{\omega}} \sim 160\ \mu$m (with $D_g = 2.185.10^5$ m^2.s^{-1}, the gaseous thermal diffusivity) is much larger than the expected bubble radius values in the reactor (ranging from some micrometres to a few tens of micrometres) within the resonance frequency range of the bubbly water filling the resonator (see Table 1). Nevertheless, to remain general, the polytropic coefficient κ is estimated at each step of the resolution, *i.e.*, for each radius range, using Devin's model [20].

Knowing the volume and pressure variations in each bubble, its compressibility can then be determined as such

$$\chi = -\frac{1}{V}\frac{\partial V}{\partial P}\Big|_S \approx -\frac{1}{V_0}\frac{\Delta V}{\Delta P}. \tag{10}$$

By considering a series combination, the total displacement can be assumed to be divided into elementary displacements absorbed by a volume change in each phase and microbubble.

2.2. Equivalent damping

The damping of individual bubbles has been already widely discussed [22-24] and is known to be due to three mechanisms: thermal exchange, radiation and viscosity. However, neither the cloud nor bubbly liquid damping coefficient are well defined in literature. Only Commander and Prosperetti [22] recommend defining a complex wave number to determine an attenuation coefficient.

In this damping-mass-spring analogy, we propose to define the equivalent damping as a parallel combination of dampers, corresponding to the damping of each bubble of the same class, in series with the equivalent damper of each class, themselves in series with a damper corresponding to the damping of the Helmholtz resonator.

This choice is motivated by the fact that the damping is directly proportional to the vibration velocity and therefore to the bubble radius. Bubbles of the same class have the same velocity, which leads

to a parallel combination of dampers. On the other hand, the velocity is different for bubbles of different radius classes, leading to a series combination of equivalent dampers of each class.

The total system damping is therefore given by

$$\delta_{eq} = \frac{b_{eq}}{m_{eff}} = \frac{1}{\frac{1}{\delta_{eq}} + \frac{1}{\delta_{eq,r}}}, \tag{11}$$

with $\delta_{eq,r}$ the equivalent damping constant of the resonator defined in [16] by the three same components, that is

$$\delta_{eq,r} = 2\frac{c_{eff}\Lambda^2}{8\pi V_c} + 2\frac{\sqrt{\omega_0}}{\sqrt{2}\,R_m}\left[\sqrt{\nu_l} + \sqrt{D_l}(\gamma - 1)\right], \tag{12}$$

where $\Lambda = S_m^2/L_e$ is the neck's acoustic conductivity, ν_l is the kinematic viscosity and D_l is the thermal diffusivity of the liquid. c_{eff} is the sound velocity of the effective medium (eq. 18), and γ is the adiabatic index.

As the study focuses on the Helmholtz resonance, *i.e.*, much lower than the bubble resonance frequency, the low-frequency approximation of bubble damping [22] is used

$$\delta_{wq} \approx 2\frac{\gamma - 1}{10\gamma}\frac{P_{atm} + \frac{2\sigma}{R_{0wq}}}{\rho_l D_g} + 4\frac{\mu_l}{\rho_l R_{0wq}^2}, \tag{13}$$

where D_g is the gaseous thermal diffusivity and μ_l the liquid dynamic viscosity.

As explained previously, to estimate the equivalent cloud damping, dampers corresponding to each single bubble of the w^{th} class of the population are organised in a parallel combination

$$\delta_w = \sum_q^{N_w} \delta_{wq}, \tag{14}$$

while the equivalent dampers of the various classes of bubbles are organised in series

$$\delta_{eq,g} = \left[\sum_w \frac{1}{\delta_w}\right]^{-1}. \tag{15}$$

3. Model validation

3.1. Methods

To check the accuracy of our microscopic modelling of the two-phase Helmholtz resonator, multiple analytical simulations of the model are performed to test its response in the linear and non-linear domains. Equation (3) is solved with a fourth-order Runge-Kutta algorithm for 5 seconds of sweep excitation in the [20 – 500] Hz range.

On the one hand, linear accuracy is examined by comparing the dependence of the resonance behaviours predicted by our model with that given by the classical homogenisation model. On the other hand, we check whether the non-linear phenomena (time amplitude desymmetrization, hysteresis, harmonic generation and softening effect) observed experimentally on a similar system in Ref. [12] are well captured by the proposed analytical model.

3.2. Linear regime

To validate the linear behaviour predicted by the proposed model based on a microscopic description of the bubble cloud, we compared the bottle's variation in linear (small excitation amplitude) resonance with the variation in the sound speed (resp. frequency) predicted by Wood's model [5]. The latter

is based on a homogenisation scheme applied to the bubbly liquid (macroscopic view), which is seen as an effective fluid or mixture characterised by effective compressibility χ_m and density ρ_m

$$\chi_m = (1-\tau)\chi_l + \tau\chi_g, \tag{16}$$

$$\rho_m = (1-\tau)\rho_l + \tau\rho_g. \tag{17}$$

Subscripts $._l$ and $._g$ correspond to the liquid and the gaseous phases respectively.

Using eq. (16) and eq. (17) and noting that gas compressibility is much higher than liquid compressibility, the effective sound velocity of the mixture c_m can be written as [25]

$$\frac{1}{c_m^2} = \rho_m \cdot \chi_m = \frac{\tau^2\kappa}{c_g^2} + \frac{(1-\tau)^2}{c_l^2} + \tau(1-\tau)\left(\frac{\rho_l}{P_0} + \rho_g\chi_l\right). \tag{18}$$

The effective velocity is then used in the Helmholtz resonance formula [26]

$$f_r = \frac{c_m}{2\pi}\sqrt{\frac{S_m}{L_e V_c}}, \tag{19}$$

to predict Wood's resonance frequency for the two-phase Helmholtz resonator.

We then compare in Table 1 the linear resonance frequency given by the proposed cloud's micro-description model to that obtained from the Wood's approximation for several two-phase populations, with different void fractions and bubble radii.

Void fraction	10^{-8}	10^{-6}	10^{-4}	10^{-2}	1
Our model for $R_0 = [1-15]$ µm	383.0 Hz	379.3 Hz	226.1 Hz	28.1 Hz	87.8 Hz
Our model for $R_0 = [1-79]$ µm	383.0 Hz	379.5 Hz	224.3 Hz	27.6 Hz	87.8 Hz
Wood model	382.3 Hz	378.2 Hz	215.2 Hz	26.1 Hz	87.6 Hz

Table 1: Linear resonance frequency predicted by the two-phase Helmholtz resonator model and with Wood's model

The good agreement reached validates our equivalent stiffness and damping modelling of the two-phase Helmholtz resonator response for small excitation amplitudes. The slight over-estimation with our model can be attributed to a stiffening issue (as observed with discretisation in the finite-element method for example).

Moreover, our modelling also reproduces well the limit case of a water single-phase ($\tau = 0$) Helmholtz resonator with a resonance at 383 Hz (382.3 Hz expected with the Helmholtz resonance formula).

3.3 Non-linear regime

Due to the lack of a non-linear model for this type of system, the non-linear response predicted by our analytical modelling cannot be compared with existing models. We therefore compare our analytical prediction with measurements and check whether the proposed model reproduces the non-linear response observed experimentally.

3.3.1 Experimental set-up

A glass bottle filled with water, acting as a Helmholtz resonator, the resonance of which is computed at 382.3 Hz (eq. 19), is used for this experimental study. The continuum cross-sectional variation in a champagne bottle is designed to avoid bubble accumulation at discontinuities and to maintain a stable void ratio. The neck cavity limit of the champagne bottle is defined by the cross-section for which a tangent to the bottle shape intersects the revolution line of the bottle's mouth [17]. The cavity radius at this point is defined by R_c as shown in Fig. 3.

The 75 cL champagne bottle is instrumented with a B&K 8103 hydrophone and a laminar microfluidic bubble generator. A B&K 4809 shaker mounted above the bottle's mouth is used to produce sweep excitation, as shown in Fig. 3.

By adjusting the pressure in the microfluidic generator, one can control the properties of the generated bubble clouds, both in terms of void fractions and radius ranges. Microfluidic generators can be optically characterised to create histogram abacus evaluating, for a given pressure, the radius histogram of the bubble population composing the cloud.

Figure 3: Experimental set-up

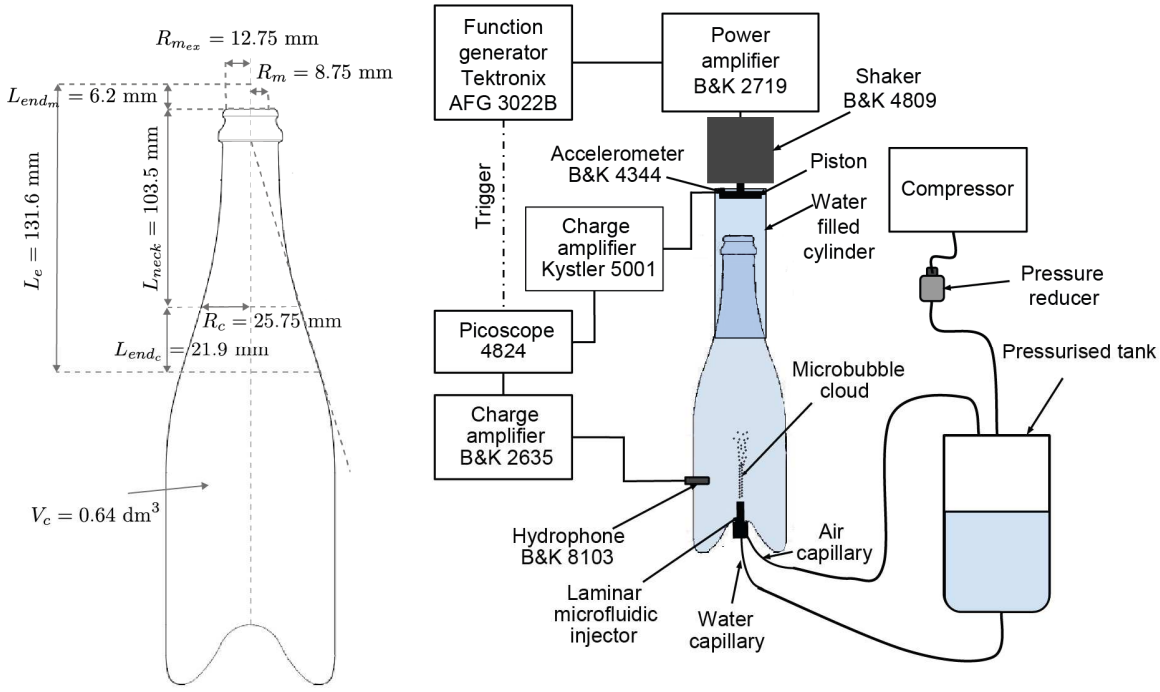

3.3.1 Experimental observation and qualitative non-linear validation

Figures 4 (a,c) show respectively the measured temporal responses and their power spectral density estimated with a Welch periodogram, for a population of radii included in the [50, 70] µm range (measured by optical camera) and an excitation amplitude ranging in [14 – 494] m.s^{-1}.

As expected, when the excitation amplitude is increased, a softening effect [13] (coupled to harmonic generation, and amplitude desymmetrisation) is observed. The sweep time is now reduced to 1 s to ensure constant cloud characteristics during the experiments. In addition, to guarantee that the void fraction remains constant during the experiment, the phase of increasing the excitation amplitude is followed by a phase of decreasing the amplitude to ensure that the same linear resonance frequency is returned. Finally, between each set of measurement, the bottle is degassed.

Thanks to Wood's model, the void fraction can be estimated by measuring the linear resonance frequency decrease due to the presence of the bubble cloud, *i.e.,* from 382.3 Hz without bubbles to 357.1 Hz, which corresponds to a void fraction of $\tau = 8.10^{-6}$.

The analytical model captures well this response as evidenced by Figs. 4 (b,d). It is worth noting here that the analytical model predicts either a softening or a hardening behaviour depending on excitation amplitude sign, as remarked by [27]. As the bubble radius, volume, internal pressure, and thus compressibility are solved in quasi-steady-state conditions (Laplace equation solved for a static excitation pressure), the model solution depends on the amplitude sign. Since it has been shown experimentally that bubbly liquid under sinusoidal sweep excitation presents a softening effect, with the resonance frequency progressively decreasing with increasing amplitude, only the softening solution was retained.

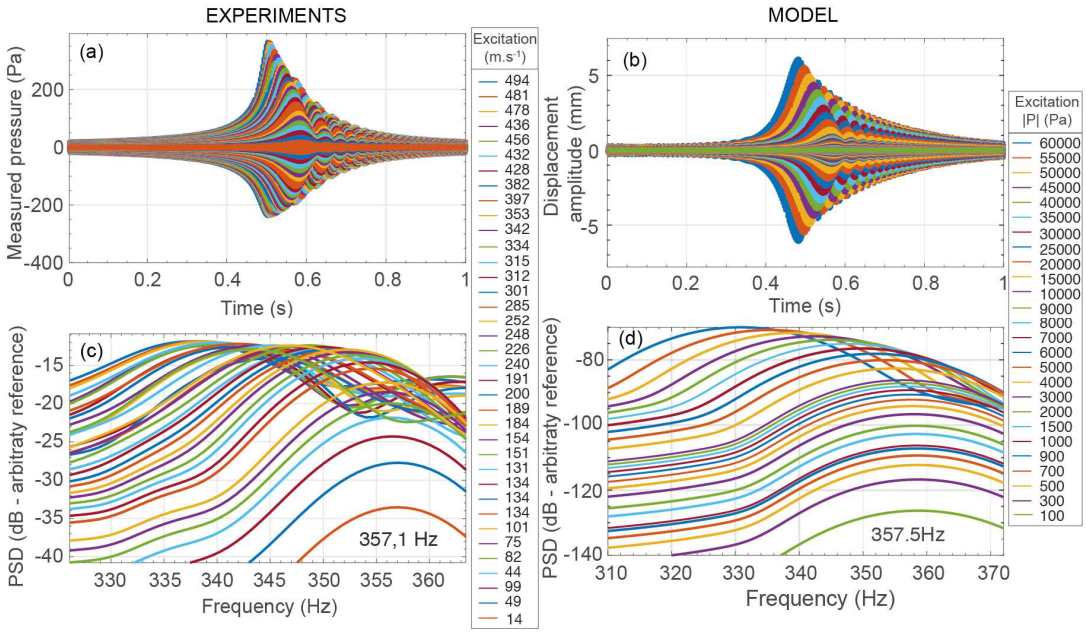

Figure 4: Measured temporal response (a) and PSD (c) of the bottle filled with bubbly water. Analytical temporal response (b) and PSD obtained with the proposed model with the microbubble cloud parameters estimated using optical characterisation and Wood's model: R_0 = 50-70 µm and $\tau = 8.10^{-6}$

3.4 Toward a Non-linear Resonant Acoustic Spectroscopy characterization

We now investigate the possibility of characterizing the cloud properties using the non-linear softening effect captured by our analytical modelling. We then test different bubble population characteristics (different void ratio, different bubble size) to see their influence on the non-linear response of the two-phase Helmholtz resonance.

Figures 5 (a-b) shows respectively the temporal and frequency responses for a bubble cloud of radii R_0 = 1-15 µm and a void fraction of $\tau = 10^{-4}$.

Figure 5: Analytical results of the model's non-linear behaviour for R_0= 1-15 µm, $\tau = 10^{-4}$:

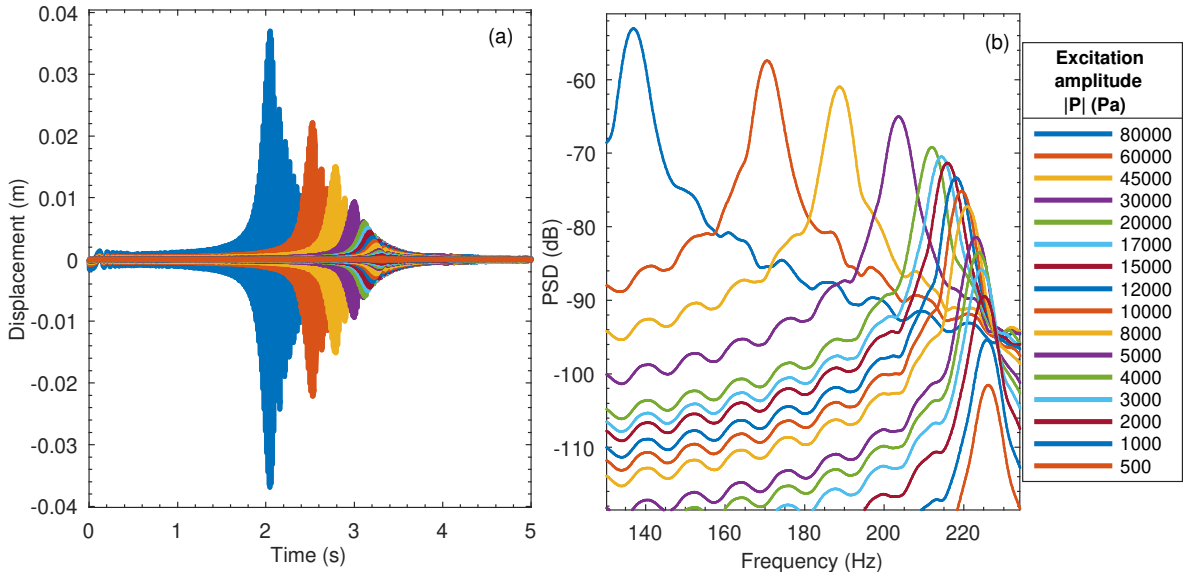

(a) temporal response and (b) power spectral density

The softening effect predicted can be quantified by applying a non-linear resonant acoustic

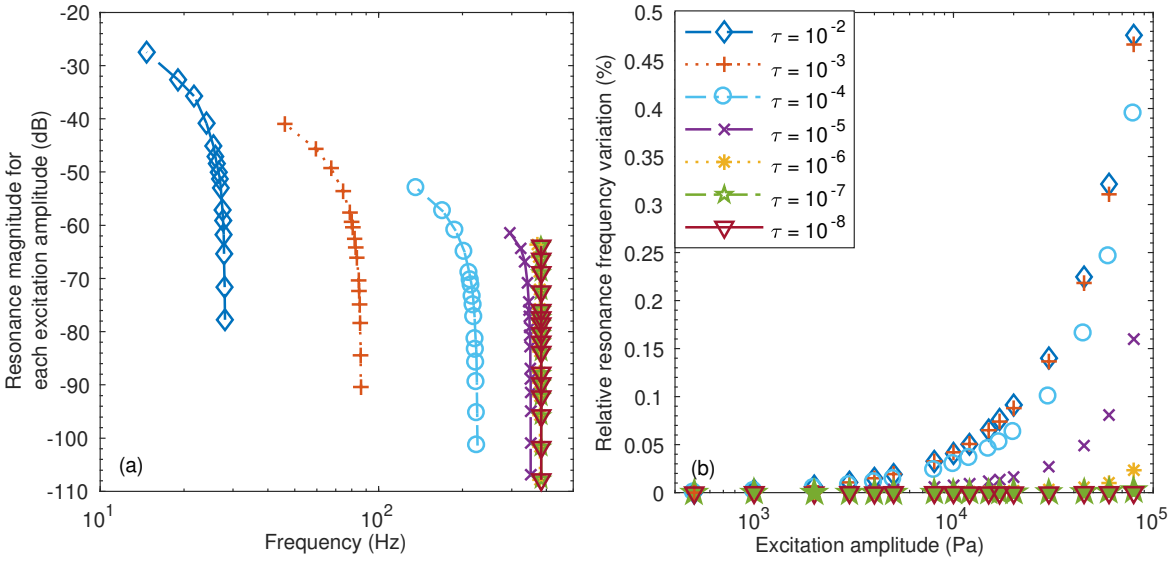

spectroscopy (NRAS) method [28], *i.e.*, by representing the relative frequency variation with the excitation amplitude and then interpolating it, as shown in Fig. 6.

Figure 6: Analytical NRAS for a bubble population of radii R_0 = 1-15 µm and a void ratio $\tau = [10^{-2}, 10^{-3}, 10^{-4}, 10^{-5}, 10^{-6}, 10^{-7}, 10^{-8}]$: (a) resonance magnitude versus frequency, (b) relative resonance frequency versus amplitude of excitation for 16 pressure levels [500, 80000] Pa

It is clear that the non-linear softening effect depends on the void ratio. The higher the void ratio, the larger the gaseous phase volume, the stronger the non-linear effect and the lower the resonance frequency.

Figure 7 shows the effect of the bubble radii on the NRAS for a monodispersed bubble cloud for a void fraction of 10^{-5}.

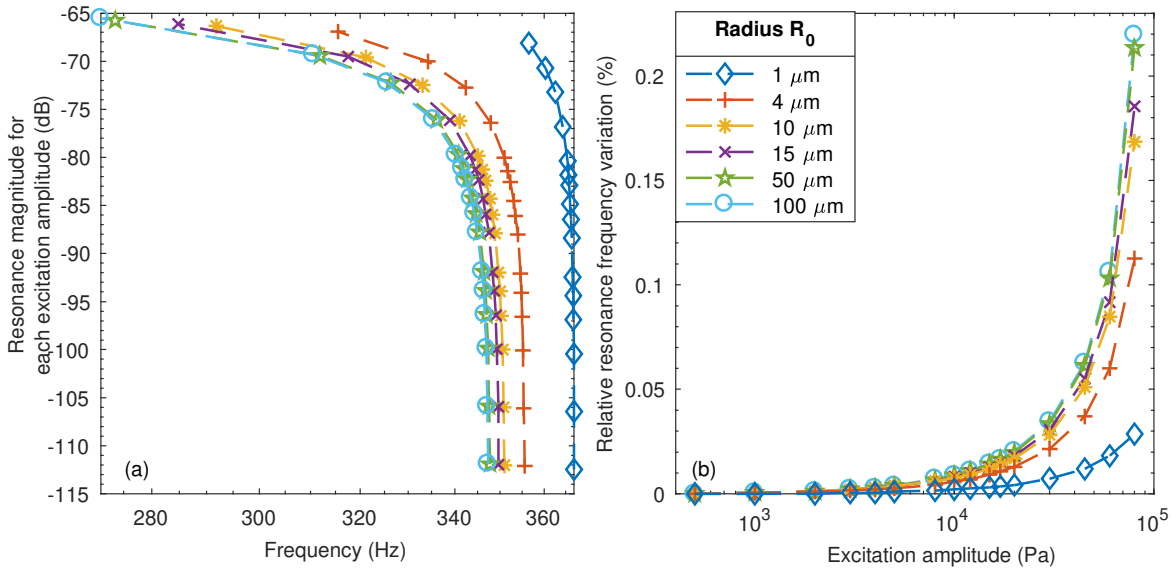

Figure 7: Analytical NRAS for $\tau = 10^{-5}$ and $R_0 = [1, 4, 10, 15, 50, 100]$ µm:
(a) resonance magnitude versus frequency, (b) relative resonance frequency versus excitation amplitude for 16 amplitudes [500, 80000] Pa

The bubble size also affects the resonant behaviour of a microbubble cloud, especially for very small radii (below 10 µm). The NRAS method is much less sensitive in the case of larger bubbles. The balance between the Laplace pressure and the atmospheric pressure (eq. 7) can explain this. For wide bubbles, the atmospheric pressure becomes predominant compared with the ratio of the surface tension to the bubble radius. In a water-air bubbly liquid, radii smaller than a few micrometres are required to achieve a balance (surface tension of water at 298.25 K is $\sigma = 0.073$), whereas the resonance behaviour of a bubbly liquid is sensitive up to 70 µm in a sodium-argon bubbly liquid (surface tension of liquid sodium at 773.25 K is $\sigma = 0.156$).

4. Conclusion and future prospects

A damped-mass-spring two-phase Helmholtz resonator model was developed to reproduce both the linear and non-linear behaviour of a bubbly resonator with the goal to study the influence of the bubble cloud parameters (radius histogram, void fraction). This model has been validated in the linear domain by comparing its resonant behaviour with that predicted by Wood's analytical model. The model is also able to predict the dependence of the non-linear effects according to the cloud histogram and the void fraction.

The results of the model have been compared with experimental measurements performed on a 75 cL champagne bottle. The bubble generation system does not make it possible to control the void fraction and population histogram separately, or to generate sufficiently small bubbles to study the relative influence of each parameter in depth. However, our experimental validation was successful. In the case of linear behaviour, good quantitative agreement was found for the resonant frequencies. In the case of non-linear behaviour, the model qualitatively estimated the overall behaviour, *e.g.* the amplitude-dependant frequency shift (softening), as well as the time and frequency response shapes.

The future prospects for this work include finding a new bubble generation system to multiply the experimental measurements (notably with small bubbles, with radii lower than 15 µm) so the experimental data can be better compared with the model's results. Other prospects include more in-depth investigation of the bubble cloud's equivalent damping, even if its impact remains small on non-linear features, as well as of the accuracy of the model to describe the other nonlinear phenomena observed experimentally: the desymmetrisation of the temporal response, the harmonic energy transfer, and hysteresis.

5. References

[1] T. Leighton, D. G. Ramble, A. D. Phelps, The detection of tethered and rising bubbles using multiple acoustic techniques, The Journal of The Acoustical Society of America 101 (5), 2626-35 (1997).

[2] M. Cavaro, C. Payan, J. Moysan, F. Baque, Microbubble cloud characterization by nonlinear frequency mixing, The Journal of the Acoustical Society of America 129 (5), EL179-EL183 (2011).

[3] M. Cavaro, A void fraction characterisation by low frequency acoustic velocity measurements in microbubble clouds, Physics Procedia 70, 496-500 (2015).

[4] L. D'Hondt, M. Cavaro, C. Payan, S. Mensah - Acoustical characterisation and monitoring of microbubble clouds - Ultrasonics 96, 10-17 (2019)

[5] A. Wood, A textbook of sound, The Macmillan company, Londres (1941).

[6] A. Prosperetti, The speed of sound in a gas–vapour bubbly liquid, Interface Focus 5, 20150024 (2015).

[7] L. Wijngaarden, Propagation of shock waves in bubble liquid mixtures, Proceedings of the International Symposium on Two-Phase Systems, 673-649 (1972).

[8] R. Caflisch, M. Miksis, G. Papanicolaou, L. Ting, Effective equations for wave propagation in bubbly liquids, Journal of Fluid Mechanics 153, 259-273 (1985).

[9] C. Payan, Caracterisation non destructive du beton : etude du potentiel de l'acoustique non lineaire, Ph.D. thesis (2007).

[10] P. Johnson, J. TenCate, R. Guyer, K. D. Abeele, Nonlinear resonant ultrasound spectrocopy, United State Patent US 6 (2001).

[11] K. Abeele, P. Johnson, R. Guyer, K. McCall, On the quasi-analytic treatment of hysteretic nonlinear response in elastic wave propagation, The Journal of the Acoustical Society of America 101 (4), 1885-1898 (1996).

[12] C. Coste, C. Laroche, S. Fauve, Acoustic resonances in a liquid with vapor bubbles: Effect of liquid-vapor transition on sound velocity and attenuation, Physical Review Letters 69 (5), 765-768 (1992).

[13] M. Cavaro, C. Payan, S. Mensah, J. Moysan, J. Jeannot, Linear and nonlinear resonant acoustic spectroscopy of micro bubble clouds, Conference paper in Proceedings of meetings on acoustics - Acoustical Society of America 16, 045003 (2012).

[14] T. Leighton, The Acoustic Bubble, Academic Press, Harcourt Brace & Company (1994).

[15] M. Alster, Improved calculation of resonant frequencies of helmholtz resonators, Journal of Sound and Vibrations 24 (1), 63-85 (1972).

[16] M. Howe, On the helmholtz resonator, Journal of Sound and Vibrations 45 (3), 427-440 (1976).

[17] A. Cummings, Acoustics of a cider bottle, Applied Acoustics 5 (3), 161-170 (1972).

[18] Y. Ando, On the sound radiation from semi-infinite circular pipe of certain wall thickness, Acta Acustica united with Acustica 22 (4), 219-225 (1969).

[19] A. Nielsen, Transaction of the Danish Academy Technical Sciences 10 (1949).

[20] C. Devin, Survey of thermal, radiation, and viscous damping of pulsating air bubbles in water, The Journal of the Acoustical Society of America 31 (12), 1654-1667 (1959).

[21] F. Bernardot, J. Bruneaux, J. Matricon, Un archetype d'oscillateur : le resonateur acoustique de helmholtz, Bulletin de l'Union des Physiciens 96, 1055-1070 (in French), (2002).

[22] K. Commander, A. Prosperetti, Linear pressure waves in bubbly liquids: Comparison between theory and experiments, The Journal of the Acoustical Society of America 85 (2), 732-746 (1989).

[23] A. Prosperetti, Thermal effects and damping mechanisms in the forced radial oscillations of gas bubbles in liquids, The Journal of the Acoustical Society of America 61 (1), 17-27 (1977).

[24] H. Medwin, Counting bubbles acoustically: a review, Ultrasonics 15 (1), 7-13 (1977).

[25] Lamarre E., Melville W.K. - *Instrumentation for the measurement of sound speed near the ocean surface* - J. Atmos. Oceanic Technol. 1995 12 pp 317 à 329.

[26] Mechel FP. Formulas of acoustics. 2nd ed. Berlin: Springer; 2008.

[27] J.-B. Doc, J.-M. Conoir, R. Marchiano, D. Fuster, Nonlinear acoustic propagation in bubbly liquids: Multiple scattering, softening and hardening phenomena, The Journal of the Acoustical Society of America 139 (4), 1703-1712 (2016).

[28] Van Damme B., Van Den Abeele K., Nonlinear Resonant Acoustic Spectroscopy. In: Ida N., Meyendorf N. (eds) Handbook of Advanced Nondestructive Evaluation. Springer, Cham (2019).

6. Acknowledgements

This work has been funded by the French Atomic Energy and Alternative Energies Commission (CEA) at Cadarache. The authors would like to acknowledge Dr. J-B. Doc for his helpful advice and patience in explaining the dual softening/hardening behaviour, as well as Verralia France for sharing the industrial drawings of their champagne bottle.